Chinese Journal of Chemistry, **2004**, *22*, 1239—1244 **Article**

n-Dodecane Hydroconversion over Nickel Supported on Different Mesoporous Aluminosilicates

FANG, Ke-Gong(房克功) REN, Jie(任杰) SUN, Yu-Han*(孙予罕)

State Key Laboratory of Coal Conversion, Institute of Coal Chemistry, Chinese Academy of Sciences, Taiyuan, Shanxi 030001, China

Several 2.0 wt% nickel catalysts supported on nanometer bimodal mesoporous aluminosilicate (NBMAS), AlHMS and AlMCM-41 were prepared by means of the wetness impregnation method. The characterization techniques such as Py-FTIR and H_2 chemisorption showed that the amount of Brönsted acid sites decreased in the order of Ni/AlHMS > Ni/AlMCM-41 > Ni/NBMAS, while the nickel dispersion differed a little. In the catalytic *n*-dodecane hydroconversion, the highest conversion was obtained over Ni/NBMAS, and the lowest isomerization selectivity occurred over Ni/AlHMS. For the cracked products, the symmetrical carbon number distribution centered at C_6 was obtained on the Ni/AlMCM-41 catalyst due to the well balanced metal/acid functions, whereas the Ni/AlHMS and Ni/NBMAS catalysts led to more C_3-C_5 and C_1+C_{11} products, respectively.

Keywords mesoporous aluminosilicate, nickel, bifunctional catalyst, *n*-dodecane hydroconversion

Introduction

The hydroconversion of *n*-paraffins is achieved over bifunctional catalysts consisting of an acidic support and a hydrogenating/dehydrogenating metal component.[1] During the reaction, the metal catalyses hydrogen transfer reactions, while isomerization and cracking occur on the Brönsted acid sites.[2,3] This reaction pathway determines that the proper ratio of metal/acid is important for the catalytic properties of the hydroconversion catalysts.

The Pt, Pd or Ni promoted zeolite or silica-alumina catalyst is the most common *n*-paraffin hydroconversion catalyst. However, its use has more or less limitations such as sensitivity to deactivation by coking or pore opening restrictions for large molecules.[4] Recently, the mesoporous materials have attracted considerable interest in separation, catalysis, *etc*.[5,6] Because of their tunable mesopore size and relatively mild acidity, these materials are very attractive supports for the bifunctional catalysts in the hydroconversion of long chain paraffins. Mokaya *et al*. reported the *n*-heptane hydroconversion over platinum-containing mesoporous molecular sieve (MMS) and found remarkable selectivity to aromatics at higher conversion levels.[1,3] Klemt *et al*. showed that the preparation technique of AlMCM-41 support was critical in controlling the product distribution when NiMo catalyst was used in *n*-decane hydrocracking.[7,8] The template removal by extraction with NH_4NO_3 ethanol solution led to an enhanced acid site density over the surface of AlMCM-41 and induced the electron deficiency state of the material, which resulted in the decrease of hydrogenolysis products. Coma and co-workers reported that the NiMo/AlMCM-41 catalyst exhibited the superior activity in the mild hydrocracking of vacuum gas oil and better selectivity toward middle distillates than NiMo/SiO_2-Al_2O_3 catalyst.[9]

In this paper, several 2.0 wt% nickel catalysts supported on nanometer bimodal mesoporous aluminosilicate (NBMAS), AlHMS and AlMCM-41 were used as catalysts for *n*-dodecane hydroconversion. The catalysts were characterized with different techniques and their catalytic properties with respect to the activity, selectivity to isomerization and carbon number distribution in the cracked products were examined.

Experimental

Catalyst preparation

Mesoporous aluminosilicate (AlMCM-41 with Si/Al=15) was hydrothermally synthesized by modifying the procedure reported in open literature.[10] Sodium aluminate (41% Al_2O_3) was dissolved in demineralised water and mixed with a certain amount of silicate anion solution (28.8% SiO_2, 10.8% Na_2O). Then the cetyltrimethylammonium bromide (CTAB) aqueous solution was added to the above mixture with stirring. Subsequently, the pH of the gel mixture was adjusted to *ca*. 10.8 by dropwise addition of 2 mol•L^{-1} HCl. The resulting gel with molar composition $1.0SiO_2$: $0.41Na_2O$: $0.033Al_2O_3$: 0.2CTAB : $100H_2O$ was transferred to a teflon-lined autoclave and aged at 393 K. After aging for 24 h, the autoclave was cooled in a wa-

* E-mail: yhsun@sxicc.ac.cn
Received January 5, 2004; revised and accepted June 14, 2004.
Project supported by the National Key Fundamental Research and Development Projects of China (No. G1999022402).

ter bath, and the pH of the gel was adjusted to 10 with the addition of 2 mol•L^{-1} HCl. The reaction gel was again aged at 393 K for an additional 24 h. The solid product recovered by filtration was washed with deionized water, dried in air at 333 K, and calcined at 873 K for 5 h to get the template-free AlMCM-41. The protonated form of AlMCM-41 was obtained by ion exchange with 1 mol•L^{-1} NH_4NO_3 solutions twice at 323 K for 8 h, dried at ambient temperature, and then calcined at 813 K for 3 h. AlHMS and NBMAS were prepared following the procedures reported in literatures.[11,12]

The nickel-supported catalysts were prepared by the wetness impregnation technique. Nickel was loaded on the support with proper amount of $Ni(NO_3)_2$ aqueous solution to get the content of 2.0 wt% Ni. After impregnation, the catalysts were vacuum-dried at 353 K for 5 h and calcined at 673 K for 4 h in air.

Characterization

The Si/Al molar ratio of the calcined mesoporous materials was determined by AES-ICP analysis. X-ray powder (XRD) measurement was carried out using a Philips PW 1050/25 diffractometer with Cu Kα radiation (50 kV, 30 mA). The textural properties of the samples were determined in a Micromeritics ASAP-2000 automated nitrogen physisorption apparatus.

Ammonia temperature-programmed desorption (NH_3-TPD) was measured by a flow system with a thermal conductivity detector. All the catalysts (150 mg) were outgassed in argon flow at 873 K for 30 min, which followed ammonia-saturation by flowing NH_3/Ar stream at 373 K for 15 min. After equilibration in argon flow for 2 h at 373 K, the catalyst was heated in a linear rate of 10 K/min to 873 K, and then the detector signal of ammonia desorption was recorded.

FT-IR spectra of pyridine adsorption were recorded on a Nicolet Magna 550 Fourier transform infrared spectrometer with 4 cm^{-1} resolution. The sample was finely ground and pressed into self-supporting wafer (10 mg/cm^2, diameter=15 mm), and then placed into the measurement cell with CaF_2 windows. Prior to pyridine sorption, the sample was evacuated at 773 K (*ca.* 1.33×10^{-2} Pa) for 4 h. The wafer was cooled to ambient temperature and a reference spectrum was collected at this temperature. Pyridine was then admitted in the sample chamber. After saturation, the cell was evacuated and a spectrum was collected at 433 K.

The temperature-programmed reduction (TPR) of the samples was performed in a flow system with a thermal conductivity detector. The samples (100 mg) were first outgassed in argon by heating to 773 K and then cooled to ambient temperature. Next, they were heated in a H_2/Ar (5/95 volumetric ratio) reducing gas mixture from room temperature to 1023 K by a heating rate of 10 K/min and the detector signal was recorded continuously.

Nickel dispersion was measured by H_2 chemisorption in a Pulse Chemisorb 2700 micrometrics. The samples were preheated at 673 K for 4 h in H_2 flow, followed by cleaning with Ar flow at 673 K for 30 min. Then the chemisorption experiments were performed at room temperature.

Catalytic test

The cumene cracking was tested using the pulse injection method. The catalysts (60 mg) loaded in a fix-bed reactor were pretreated *in situ* by heating at 673 K for 2 h in argon with flow rate of 40 mL/min. Then 0.2 mL of reactant was injected into the catalyst bed at given temperature. The products were analyzed on line by a gas chromatograph equipped with a flame-ionization detector.

n-Dodecane hydroconversion was carried out in a down flow fixed-bed stainless steel tube reactor (i.d=6 mm; 120 cm in length) at 2.0 MPa and H_2/*n*-dodecane molar ratio of 20. The catalyst was pretreated in Ar flow and then reduced *in situ* in a flow of H_2 at 673 K for 4 h prior to the start of the reaction. The gas products were analyzed by gas chromatograph with a GDX-103 column and FID detector, an OV-101 capillary column and FID detector for the liquid ones.

Results and discussion

Structural characterization

Figure 1 shows the XRD patterns of the samples. All the supports displayed a single broad (100) peak, similarly to those of the comparable mesoporous materials.[11-13] The materials exhibiting such single peak XRD patterns have been reported to possess short-range hexagonal symmetry.[14,15] After nickel loading, the (100) peak for the three supports became broaden and its intensity decreased, suggesting that the distortion of the mesostructure took place. The composition and textural properties of the samples are listed in Table 1. The Si/Al ratios of the mesoporous supports determined by AES-ICP analysis were close to those of the reactant gels. The AlMCM-41 and AlHMS showed high surface area and a single mesopore size distribution. By contrast, the NBMAS displayed low surface area due to the lower hexagonal order.[12] In addition, the special bimodal pore size distribution could be observed for NBMAS sample. The pore size at 2.28 nm was assigned to the ordered hexagonal mesopores formed by the templating function of surfactant micelles, while the larger pore size at 97.3 nm was coincided with the inter-particle pores created by the aggregation of the crystallites. Upon nickel incorporation, the surface area, pore volume and pore size decreased for the AlMCM-41 and AlHMS due to the hydrotreatment and nickel-support interaction after nickel impregnation, which was similar to the results reported elsewhere.[9,16,17] In the case of NBMAS sample,

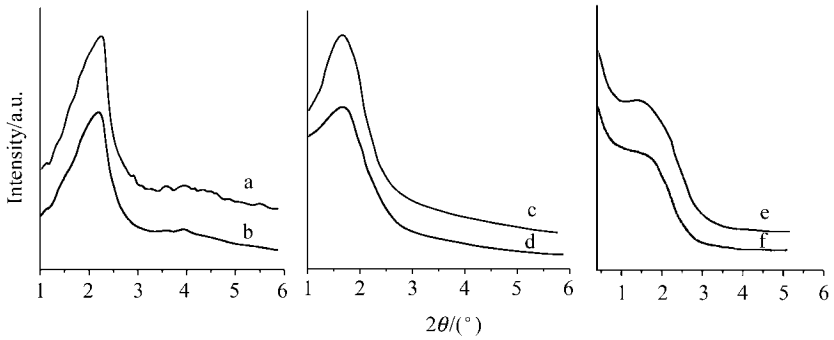

Figure 1 Powder XRD patterns of the samples. (a) AlMCM-41; (b) Ni/AlMCM-41; (c) AlHMS; (d) Ni/AlHMS; (e) NBMAS; (f) Ni/NBMAS.

Table 1 Textural properties of the Ni-supported catalysts

Catalyst	Si/Al ratio		S_{BET}/	V_{pore}/	R^a/nm	
	Gel	Crystal	($m^2 \cdot g^{-1}$)	($cm^3 \cdot g^{-1}$)	R_1	R_2
AlMCM-41	15	15.8	885.3	0.80	2.49	—
Ni/AlMCM-41	—	—	877.7	0.78	2.43	—
NBMAS	15	13.9	411.6	0.68	2.28	97.3
Ni/NBMAS	—	—	380.4	0.59	2.25	35.5
AlHMS	15	14.7	819.4	0.66	2.58	—
Ni/AlHMS	—	—	786.8	0.54	2.56	—

[a] *R*: Pore diameter calculated from the N_2 adsorption branch.

the second pore size decreased heavily but surface area and pore volume decreased a little. This could be explained as follows. For the mesoporous molecular sieves, the hexagonal mesopores mainly contributed to the surface area and pore volume according to the BJH method used in N_2 sorption. However, the second pores of the NBMAS were assigned to the inter-particle pores, which were not the real structural pores. Therefore, the effect of the second pore on the surface area and pore volume is small. After nickel impregnation and calcinations, the second pore size decreased heavily, indicating that the crystal particles aggregated more closely.

Acidity

The NH_3-TPD profiles are shown in Figure 2. All the catalysts exhibited the weak and medium acid peaks, centered at *ca*. 485—500 K and *ca*. 570 K, respectively. The total acid number decreased in the order of Ni/NBMAS > Ni/AlMCM-41 > Ni/AlHMS (see Table 2). More concretely, the amount of weak and medium acid sites was nearly equal over Ni/AlMCM-41 and Ni/NBMAS catalysts, while Ni/AlHMS contained a larger fraction of medium acid sites. Besides, a small desorption peak centered at 670 K could be observed in the NH_3-TPD of Ni/NBMAS, which might be consistent with the strong Lewis acidity created by the extra-framework Al species. This result suggested that there were higher proportion of extraframework Al species located at or near the pore wall surface for NBMAS than that for AlMCM-41 and AlHMS. Similar phenomena were also reported by Ryoo *et al.*[19] when they prepared the mesoporous metallosilicates via post-synthetic metal implantation.

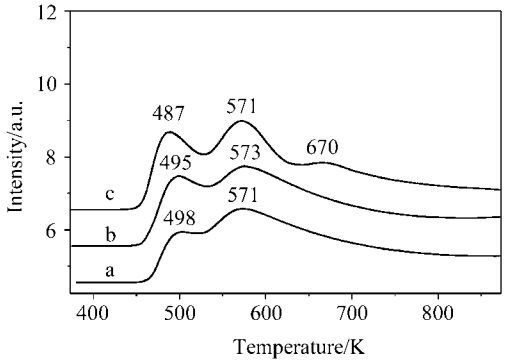

Figure 2 NH_3-TPD curves of the catalysts. (a) Ni/AlHMS; (b) Ni/AlMCM-41; (c) Ni/NBMAS.

Table 2 Acidity and metal properties of Ni-supported catalysts

Catalyst	Acidity[a]/ (mmol Py•g^{-1})			NH_3 desorbed[b]/ ($mmol \cdot g^{-1}$)	D_{Ni}[c]/ %	n_{Ni}/n_A[d]
	B	L	B+L			
Ni/NBMAS	0.30	1.21	1.51	0.71	10.0	0.11
Ni/AlMCM-41	0.52	0.88	1.40	0.62	11.1	0.07
Ni/AlHMS	0.71	0.66	1.37	0.57	10.7	0.05

[a] Calculated using the extinction coefficients by Emeis;[18] [b] NH_3 desorbed beyond 373 K; [c] Nickel dispersion; [d] The ratio of exposed nickel atom number to the Brönsted acid number.

Py-FTIR spectra and the quantitative calculation of the acid sites are given in Figure 3 and Table 2. The bands at 1453 and 1550 cm^{-1} (representing Lewis acid and Brönsted acid, respectively) were observed for all the catalysts (Figure 3). The sequence of the total amount of Brönsted and Lewis acid sites with respect to the catalysts was consistent with the NH_3-TPD results. The Ni/AlHMS showed the larger amount of Brönsted acid sites, while the Ni/NBMAS contained a smaller amount of Brönsted acid sites and larger Lewis acid sites (Table 2). For further comparing the Brönsted

acidity of the catalysts, the cumene cracking reaction was chosen as a probe to measure the Brönsted acidity of the catalysts. Generally, the higher the cumene conversion was, the larger the amount of Brönsted acid sites present on the surface of the catalyst.[20] The activities of the catalysts were in the order of Ni/AlHMS > Ni/AlMCM-41 > Ni/NBMAS (Table 3), which mirrored the acidity obtained from the Py-FTIR analysis.

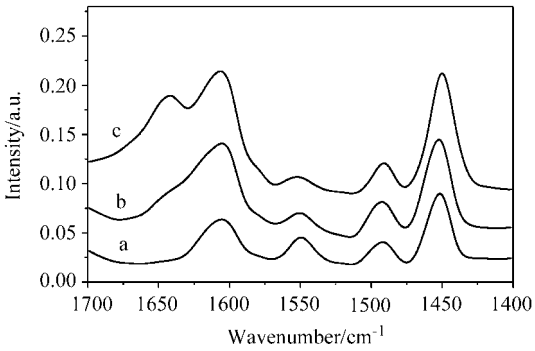

Figure 3 Py-FTIR spectra of pyridine adsorbed on the samples after being degassed at 433 K. (a) Ni/AlHMS; (b) Ni/AlMCM-41; (c) Ni/NBMAS.

Table 3 Activities for cumene cracking reaction

Catalyst	Cumene conversion/%		
	523 K	573 K	623 K
Ni/AlMCM-41	5.3	26.4	54.1
Ni/NBMAS	3.2	13.1	40.1
Ni/AlHMS	10.7	30.7	62.2

Surface metal function

All the catalysts exhibited two reduction stages (Figure 4), similarly to that reported elsewhere.[21] The low temperature reduction stage coincided with the reduction of Ni-oxide (most free nickel oxide with a bulk character), whereas the second reduction stage originated from the reduction of the small nickel oxide species, chemically bounded with the framework of the mesostructure. For the Ni/AlMCM-41 catalyst, the low temperature peak was very small, shouldered with the broad high temperature peak maximum at 847 K, indicating that the Ni/AlMCM-41 catalyst mainly contained small nickel oxide particles, which had strong interaction with the support. By contrast, the Ni/AlHMS and Ni/NBMAS demonstrated an intense low temperature peak and the high temperature reduction peak shifted to the lower temperature (maximum at 819 and 798 K, respectively), suggesting that there were more large NiO particles on the surface of the Ni/AlHMS and Ni/NBMAS catalysts and the nickel-support interaction was weaker than that of Ni/AlMCM-41 catalyst.

The nickel dispersion of the Ni/AlMCM-41 catalysts determined by hydrogen chemisorption is presented in Table 2. The nickel dispersions of the catalysts differed a little, though the degressive sequence of Ni/AlMCM-41 > Ni/AlHMS > Ni/NBMAS also could be observed. The quantitative calculation results of metal/acid ratio (n_{Ni}/n_A) over the catalysts based on the Py-FTIR analysis and hydrogen chemisorption are listed in Table 2, from which it could be seen that the metal/acid ratio increased in the order of Ni/AlHMS < Ni/AlMCM-41 < Ni/NBMAS.

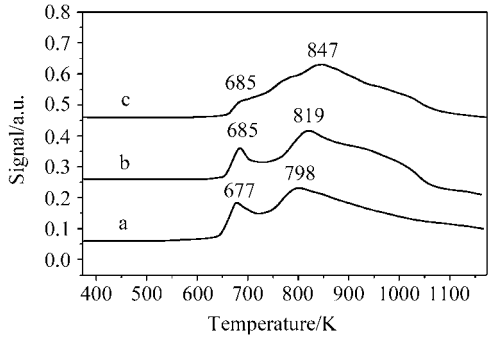

Figure 4 H_2-TPR profiles of the catalysts. (a) Ni/NBMAS; (b) Ni/AlHMS; (c) Ni/AlMCM-41.

Catalytic performance

The conversion of *n*-dodecane over the bifunctional catalysts versus reaction temperature was given in Figure 5. At the reaction temperature range of 573—593 K, the activity of Ni/AlHMS was very close to that of Ni/AlMCM-41. As the temperature further increased, the activity of Ni/AlHMS was elevated faster than that of the latter. Combined with the characterization results of the acidity, it could be concluded that the effect of the Brönsted acidity on the *n*-dodecane conversion was more apparent at higher temperature. The more the Brönsted acid sites was, the more *n*-dodecane could be converted over the catalyst. From Figure 5, it was also observed that the conversion of *n*-dodecane over Ni/NBMAS catalyst was always higher than those over Ni/AlHMS and Ni/AlMCM-41 catalysts at the whole reaction temperature range. This was not consistent with the Brönsted acid number over the catalysts. Over the Ni/NBMAS catalyst, the metal function override the acid one, causing the hydrogenolysis reaction occurred on

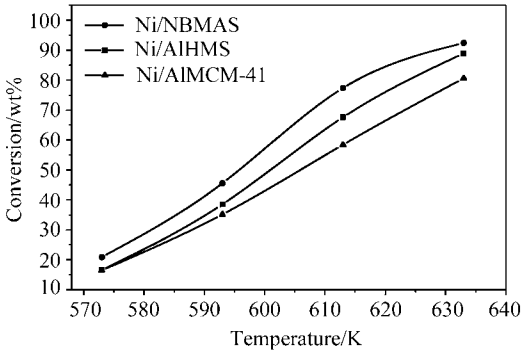

Figure 5 *n*-Dodecane conversion as a function of temperature over the catalysts.

the metal sites of Ni/NBMAS catalyst. Thus, such hydrogenolysis reaction consumed a part of *n*-dodecane, which ultimately contributed to the highest *n*-dodecane conversion. Besides, the inter-particle pores in the structure of NBMAS favored the diffusion of *n*-dodecane, which might also facilitate the conversion of *n*-dodecane in some extent.

The selectivity toward *iso*-dodecane over the three catalysts decreased with the increase of conversion (Figure 6), which was commonly observed in the hydroisomerization-cracking of *n*-paraffins. However, the isomerization selectivity was higher for Ni/NBMAS and Ni/AlMCM-41 as compared to that for Ni/AlHMS. Considering the proposed bifunctional reaction mechanism for hydroisomerization and hydrocracking,[22-24] the balance between metal and acid functions should have great influence on the isomerization selectivity. The higher the metal/acid ratio (n_{Ni}/n_A) was, the stronger (de)hydrogenating capacity would be obtained over the catalyst. Over the Ni/NBMAS and Ni/AlMCM-41 catalysts, the primary carbenium ions could be rapidly transferred to the metal sites without further being cracked due to the higher metal/acid ratio of the catalysts, therefore the higher isomerization selectivity was obtained.

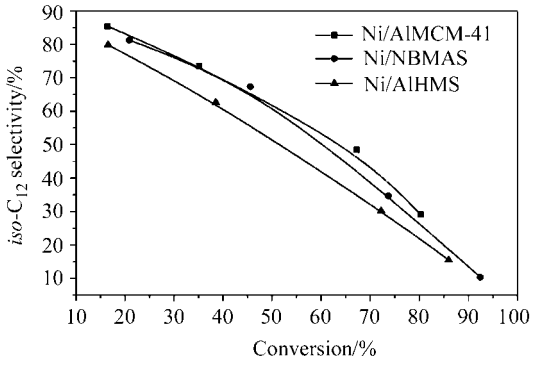

Figure 6 Isomerization selectivity as a function of *n*-dodecane conversion.

Figure 7 gives the carbon number distribution of the cracked products at conversion of *ca.* 45%. The Ni/AlMCM-41 showed nearly symmetrical distribution centered at C_6, indicating that the metal and acid functions were well balanced over the catalyst and *n*-dodecane performed an ideal hydroisomerization-cracking behavior. By contrast, the imbalance of metal/acid functions caused more C_3-C_5 and C_1+C_{11} products obtained over the Ni/AlHMS and Ni/NBMAS catalysts, respectively.

Conclusions

The 2.0 wt% nickel catalysts supported on NBMAS, AlHMS and AlMCM-41 showed different performances. The amount of Brönsted acid sites decreased in the order of Ni/AlHMS＞Ni/AlMCM-41＞Ni/NBMAS, while

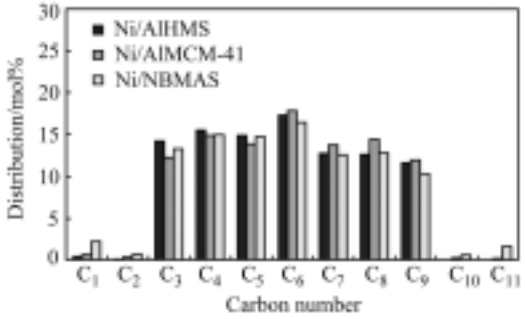

Figure 7 Carbon number distribution of the cracked products over the catalysts at *n*-dodecane conversion of *ca*. 45%.

the nickel dispersion differed a little. The hydrogenolysis reaction occurred on the Ni/NBMAS contributed to the highest *n*-dodecane conversion, and the largest amount of Brönsted acid sites resulted in the lowest isomerization selectivity over the Ni/AlHMS catalyst. For the cracked products, the Ni/AlMCM-41 catalyst exhibited the symmetrical carbon number distribution centered at C_6 due to the well balanced metal/acid functions, whereas the imbalance between metal and acid functions of the Ni/AlHMS and Ni/NBMS catalysts caused more C_3-C_5 and C_1+C_{11} products, respectively.

References

1 Mokaya, R.; Jones, W.; Moreno, S.; Poncelet, G. *Catal. Lett.* **1997**, *49*, 87.
2 Coonradt, M. L.; Garwood, W. E. *Ind. Eng. Chem. Prod. Res. Dev.* **1964**, *3*, 38.
3 Elangovan, S. P.; Bischof, C.; Hartmann, M. *Catal. Lett.* **2002**, *80*, 35.
4 Coma, A.; Martinez, A.; Pegher, S.; Perego, C.; Bellusi, G. *Appl. Catal. A* **1997**, *152*, 107.
5 Kersge, C. T.; Leonowicz, M. E.; Roth, W. J.; Vartuli, J. C.; Beck, J. S. *Nature* **1992**, *359*, 710.
6 Mokaya, R.; Jones, W.; Luan, Z.; Alba, M. D.; Klinowski, J. *Catal. Lett.* **1996**, *37*, 113.
7 Klemt, A.; Taouli, A.; Koch, H.; Reschetilowski, W. *Stud. Surf. Sci. Catal*. **1999**, *127*, 405.
8 Trong On, D.; Desplantier, G. D.; Danumah, C.; Kaliaguine, S. *Appl. Catal. A* **2001**, *222*, 299.
9 Coma, A.; Martinez, A.; Martinez, S. V.; Monton, J. B. *J. Catal*. **1995**, *153*, 25.
10 Pauly, T. R.; Petkov, V.; Liu, Y.; Billinge, S. J. L.; Pinnavaia, T. J. *J. Am. Chem. Soc.* **2002**, *124*, 97.
11 Tanev, P. T.; Pinnavaia, T. T. *Chem. Mater.* **1996**, *8*, 2068.
12 Zhang, Y.; Wu, D.; Sun, Y. H.; Peng, S. Y. *J. Fudan Univ.* **2002**, *41*, 264 (in Chinese).
13 Chen, X.; Huang, L.; Ding, G.; Li, Q. *Catal. Lett.* **1997**, *44*, 123.
14 Tanev, P. T.; Chibwe, M.; Pinnavaia, T. T. *Nature* **1994**, *368*, 321.
15 Schmidt, R.; Akporiaye, D.; Stocker, M.; Ellestad, O. H. In *Zeolites and Related Materials, State of the Art 1994, Stud. Surf. Sci. Catal*. Vol. 84, Elsevier, Amsterdam, **1994**, p. 61.

16 Lewandowska, A.; Monteverdi, S.; Bettahar, M.; Ziolek, M. *J. Mol. Catal. A* **2002**, *188*, 85.
17 Song, C. S.; Reddy, K. M. *Appl. Catal. A* **1996**, *176*, 1.
18 Emeis, C. A. *J. Catal.* **1993**, *141*, 347.
19 Ryoo, K.; Jun, S.; Kim, J. M.; Kim, M. J. *Chem. Commun.* **1997**, 2225.
20 Mokaya, R.; Jones, W. *Chem. Commun.* **1997**, 2185.
21 Lensveld, D. J.; Gerbrand, J.; Dliien, A. J.; Jong, K. P. *Microporous Mesoporous Mater.* **2001**, *44—45*, 401.
22 Weitkamp, J. *Ind. Eng. Chem. Prod. Res. Dev.* **1982**, *21*, 550.
23 Conradt, M. L.; Garwood, W. E. *Ind. Eng. Chem. Prod. Res. Dev.* **1981**, *20*, 654.
24 Weisz, P. B. *Adv. Catal.* **1962**, *13*, 137.

.

(E0401058 CHENG, B.)